Supplemental Information—Imaging via Correlation of X-ray Fluorescence Photons

Fabian Trost, Kartik Ayyer, Mauro Prasciolu, Holger Fleckenstein, Miriam Barthelmess, Oleksandr Yefanov, J. Lukas Dresselhaus, Chufeng Li, Saša Bajt, Jerome Carnis, Tamme Wollweber, Abhishek Mall, Zhou Shen, Yulong Zhuang, Stefan Richter, Sebastian Karl, Sebastian Cardoch, Kajwal Kumar Patra, Johannes Möller, Alexey Zozulya, Roman Shayduk, Wei Lu, Felix Braue, Bertram Friedrich, Ulrike Boesenberg, Ilia Petrov, Sergey Tomin, Marc Guetg, Anders Madsen, Nicusor Timneanu, Carl Caleman, Ralf Röhlsberger, Joachim von Zanthier, and Henry N. Chapman

I. FLUORESCENCE DETECTION

The angularly-resolved fluorescence was detected in the forward direction with the AGIPD [1] placed 8 m downstream of the Cu foil. For all measurements, the detector was operated in its high-gain state, where it has an energy resolution of about 1 keV and so can detect single photons but cannot completely distinguish 8.04 keV Cu Kα fluorescence from 8.91 keV Cu Kβ fluorescence, nor from the 9.00 keV elastically scattered photons. To suppress the unwanted photons, a 20 µm-thick Ni filter was placed 700 mm downstream of the Cu foil. This transmitted 0.8% of the elastic photons, 0.4% of the Cu Kβ, and 43% of the Cu Kα. A He-filled flight tube placed between the Cu and Ni foils reduced air absorption of the fluorescence and a beamstop was located just downstream of the Ni foil to block the remaining direct beam.

The finest interference fringes in a speckle pattern are formed by emission originating from the extreme positions of the fluorescing structure. The recovery of an image of a compact object from a map of $|F(\vec{q})|^2$ therefore requires that patterns are recorded with a fine enough angular resolution to achieve Nyquist sampling of those fringes. The AGIPD, with a pixel width of 200 µm, was placed 8 m downstream of the Cu foil to provide sufficient sampling for objects up to 6 µm extent at $\lambda = 1.54$ (the wavelength of Cu Kα fluorescence). This detector was located at the end of a vacuum flight tube with a diamond entrance window located just downstream of the Ni foil and beamstop. The combined transmissions of the foils, the air, the 700 µm thick diamond window, a 25 µm thick Kapton entrance window of the He flight tube, and the detector quantum efficiency, gave an overall detection efficiency of 0.135.

II. PHASE RETRIEVAL

An image of the fluorescence emitter distribution was obtained by phasing the measured $|g^{(1)}|$ map (see Fig. 3a). The simplest iterative phase retrieval algorithm, "error reduction, alternatively enforces the Fourier transform magnitude of the estimated image to be equal to $|F|$, and the structure to be less than a given size or shape called the support [2]. We used a variation of the "Shrinkwrap" algorithm [3] in which the support region is determined from the N strongest pixels of a blurred version of the current iterate. The support was updated on each iteration. The number of pixels in the support was initially set to $N = 450$ and the blurring utilized a Gaussian kernel with a width σ that was initially set to 4 pixels. In addition, we constrained the real-space image ρ to be real and positive. Starting with random Fourier phases, iterations alternated between "error reduction" and the "difference map algorithms [4]. This process was repeated 200 times during which the support area shrank to an area of $N = 300$ pixels, and the Gaussian smoothing kernel size shrank to $\sigma = 0.25$ pixels. The "difference map" algorithm avoids local minima using a combination of constraint operations that reaches a fixed point at the solution [4]. To further reduce the possibility of local minima, the "hybrid input-output" algorithm [2] was used in iterations 25, 50, 75, 100, and 125. In Fig. S1a the normalized RMS error [5] is plotted as a function of iterations for 6 randomly chosen phase retrievals. The metric is defined by

$$E_n^2 = \frac{\sum_{x,y} \left| f_n(x,y) - |g^{(1)}(x,y)| \right|^2}{\sum_{x,y} \left| g^{(1)}(x,y) \right|^2}, \tag{S1}$$

where f_n denotes the Fourier amplitudes of the n^{th} iterate and $|g^{(1)}(x,y)|$ the measured amplitudes.

In the presence of noise, a reliable image estimate can be obtained by averaging many trials of the above procedure [6]. We computed 1000 such estimates, each from a different random start. Our real-space operation of selecting the 450 strongest pixels does not constrain the position of the structure, nor does it distinguish between an image and its centrosymmetric inverse. We therefore brought each estimate into a common alignment and orientation by correlation to a reference estimate prior to averaging [5]. To demonstrate the convergence, we determined the standard deviation achieved for different numbers of averages. Fifty sets of real-space image estimates were computed and in each set we averaged n of these estimates, to give averages $\langle \rho_m(x,y) \rangle_n$. The normalized RMS error σ_n is then defined by

$$\sigma_n^2 = \frac{\sum_{x,y} \frac{1}{50} \sum_{m=1}^{50} \left| \langle \rho_m(x,y) \rangle_n - \langle \rho_m(x,y) \rangle_{n,m} \right|^2}{\sum_{x,y} \left| \langle \rho_m(x,y) \rangle_{n,m} \right|^2}, \tag{S2}$$

where $\langle \rho_m(x,y) \rangle_{n,m}$ denotes the average of all 50 averaged estimates. This normalised standard deviation is plotted in Fig. S1b as a function of the number of averages, n.

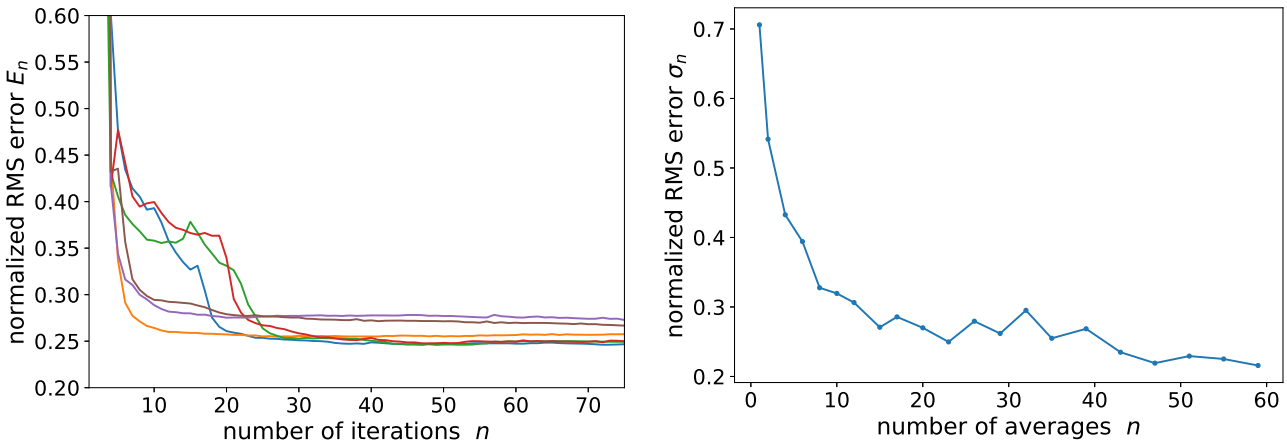

(a) (b)

FIG. S1: **(a)** Normalized RMS error as a function of iterations for 6 randomly chosen retrievals. **(b)** Normalized RMS error of the average of individual iterates, defined by Eq. (S2).

[1] A. Allahgholi, J. Becker, A. Delfs, R. Dinapoli, P. Goettlicher, D. Greiffenberg, B. Henrich, H. Hirsemann, M. Kuhn, R. Klanner, A. Klyuev, H. Krueger, S. Lange, T. Laurus, A. Marras, D. Mezza, A. Mozzanica, M. Niemann, J. Poehlsen, J. Schwandt, I. Sheviakov, X. Shi, S. Smoljanin, L. Steffen, J. Sztuk-Dambietz, U. Trunk, Q. Xia, M. Zeribi, J. Zhang, M. Zimmer, B. Schmitt, and H. Graafsma, J. Synchr. Rad. **26**, 74 (2019).

[2] J. R. Fienup, Appl. Opt. **21**, 2758 (1982).

[3] S. Marchesini, H. He, H. N. Chapman, S. P. Hau-Riege, A. Noy, M. R. Howells, U. Weierstall, and J. C. H. Spence, Phys. Rev. B **68**, 140101 (2003).

[4] V. Elser, J. Opt. Soc. Am. A **20**, 40 (2003).

[5] J. R. Fienup, Appl. Opt. **36**, 8352 (1997).

[6] D. Shapiro, P. Thibault, T. Beetz, V. Elser, M. Howells, C. Jacobsen, J. Kirz, E. Lima, H. Miao, A. M. Neiman, *et al.*, Proc. Nat. Acad. Sci. USA **102**, 15343 (2005).